Biochimica et Biophysica Acta 1807 (2011) 510–517

Contents lists available at ScienceDirect

Biochimica et Biophysica Acta

journal homepage: www.elsevier.com/locate/bbabio

On understanding proton transfer to the biocatalytic [Fe—Fe]$_H$ sub-cluster in [Fe—Fe] H_2ases: QM/MM MD simulations

G. Hong [a,b], A.J. Cornish [c], E.L. Hegg [c], R. Pachter [a,*]

[a] Air Force Research Laboratory, Materials and Manufacturing Directorate, Wright-Patterson Air Force Base, OH 45433, USA
[b] General Dynamics Information Technology, Dayton, OH 45431, USA
[c] Michigan State University, East Lansing, MI 48824, USA

ARTICLE INFO

Article history:
Received 9 July 2010
Received in revised form 26 January 2011
Accepted 31 January 2011
Available online 4 February 2011

Keywords:
Fe—Fe
Hydrogenases
QM/MM MD simulation
Proton transfer
Hydrogen production activity

ABSTRACT

Proton transfer to the [Fe—Fe]$_H$ sub-cluster in the *Desulfovibrio desulfuricans* (DdH) and *Clostridium pasteurianum* (CpI) [Fe—Fe] hydrogenases was investigated by a combination of first principles and empirical molecular dynamics simulations. Pathways that can be inferred from the X-ray crystal structures of DdH and CpI, i.e., (Glu159 → Ser198 → Glu156 → water460 → Cys178 → DTMA([Fe—Fe]$_H$) and (Glu282 → Ser319 → Glu279 → water612 → Cys299), respectively, were considered. Proton transfer from Cys178 to DTMA in the [Fe—Fe]$_H$ sub-cluster in DdH was readily observed in our results, specifically when [Fe—Fe]$_H$ was in the reduced state ([Fe^I—Fe^I]) or in the mixed valence state for the protonated distal iron Fe$_d$ ([Fe^I—Fe^{II}—H$^-$]$_H$). A concerted mechanism is proposed, where proton transfer in DdH from Glu159 to Glu156 via Ser198 and Glu156 to Cys178 via water460 readily occurred, as well as from Glu282 to Glu279 via Ser319 and Glu279 to Cys299 via water612 in CpI. The theoretical prediction of the proton transfer characteristics is consistent with the assumed biocatalytic mechanism of the [Fe—Fe] hydrogenases in which the proton binds at Fe$_d$, providing confirmation that has not been explored so far. The computational results were qualitatively validated by the agreement with experimental hydrogen production activity data for mutated CpI enzymes, relative to the wild-type protein. Finally, the insight provided by the simulations, combined, in part, with experimental validation, are important for establishing an approach in future exploration of proton transfer to the active site in this class of enzymes, and possibly also for biomimetic analogs.

Published by Elsevier B.V.

1. Introduction

Hydrogenases (H_2ases) are metalloenzymes used by microorganisms to catalyze hydrogen production and consumption [1]. This class of enzymes is subdivided by the active sites [2], namely, [Ni—Fe] [3], [Fe—Fe] [4,5], and [Fe] H_2ases [6]. [Fe—Fe] H_2ases are efficient in hydrogen production, for instance, under optimal conditions, it was estimated that each molecule of *Desulfovibrio desulfuricans* (DdH) and *Clostridium pasteurianum* (CpI) can produce 9000 and 6000 molecules of hydrogen per second [7,8], respectively. Indeed, the efficiency of [Fe—Fe] H_2ases [9] triggered extensive research both theoretically and experimentally [10–14]. The determination of the X-ray crystal structures of CpI [4] and DdH [5] revealed common structural features, specifically a [6Fe—6 S] active site cluster (H-cluster, HC), comprised of a [Fe—Fe] sub-cluster (2 CN and 3 CO groups, and a bridging ligand) and a [4Fe—4 S] sub-cluster, covalently linked by a Cys thiolate. The bridging ligand in the sub-cluster of DdH is assumed to consist of di-thiomethylamine (DTMA) [15], as supported by a ^{14}N HYSCORE study [16]. Recently, a refined CpI crystal structure suggested a di-thiomethyl ether bridging ligand [17]. Oxidation states were investigated by electron paramagnetic resonance (EPR) [18] and infrared (IR) [19], including an EPR-silent catalytically inactive state H_{ox}^{air}, an EPR-accessible mixed-valence state H_{ox}, and an EPR-silent reduced state H_{red}. [4Fe—4 S] was assigned an EPR-silent [4Fe—4 S]$^{2+}$ state. Two alternative formal charges of the di-iron sub-cluster were consistent with Mössbauer data [20], namely [Fe^{II}—Fe^{II}] for H_{ox}^{air}, [Fe^I—Fe^{II}] for H_{ox}, and [Fe^I—Fe^I] for H_{red}; or [Fe^{III}—Fe^{III}] for H_{ox}^{air}, [Fe^{II}—Fe^{III}] for H_{ox}, and [Fe^{II}—Fe^{II}] for H_{red}. The former supposition was supported by IR spectra [21] of model compounds, in agreement with theoretical investigations [22–25], as calculated vibrational frequencies based on the latter supposition were systematically too large compared to experiment, attributed to dependence of the CO ligands on the electron density at the metal center [26]. Recent Q-band ^{57}Fe-ENDOR and HYSCORE studies of DdH [27], as well as computational studies [8,22,23,28–32], also supported the first supposition. Thus, the former charge scheme was assumed in the present computational investigation.

Hypotheses on the catalytic cycle have differed in early work. Based on DTMA as the bridging ligand [22–24,28,29,32], it was postulated that H_2 or H^+ bind at the distal iron atom Fe$_d$. This

* Corresponding author.
E-mail address: Ruth.Pachter@wpafb.af.mil (R. Pachter).

0005-2728/$ – see front matter. Published by Elsevier B.V.
doi:10.1016/j.bbabio.2011.01.011

mechanism was most recently further assumed plausible even for dithiomethylether as the bridging ligand [33]. Alternatively, H_2 or H^+ could bind to both Fe atoms in a bridged position [30,31,34]. However, the former mechanism was also supported by the observation that in the DdH crystal structure a CO ligand is in the semi-bridging position amid the irons in $[Fe—Fe]_H$, leaving a vacant binding site at Fe_d [5]. Moreover, the calculated barrier of proton transfer from DTMA to Fe_d for the model compound $[Fe_2(S_2C_2H_4)(\mu\text{-}CO)(H)(CO)(PMe_3)_4]^+$ is low, and the terminal hydride can be more reactive than a bridging hydride [35]. Note that di-iron clusters favor the conformation where the CO is in a terminal position [34], forming a bridged hydride upon protonation [32,36]. Recent calculations that included the effects of the protein environment [37] have further supported this mechanism. However, proton transfer to the active site [38] in this case was not examined, except for model compounds [39].

In this work, based on DTMA as the bridging ligand, and the mechanism in which the distal iron binds the proton, most consistent with previous experimental and theoretical studies, we investigated proton transfer characteristics from Cys178 to DTMA of $[Fe—Fe]_H$ in DdH, as well as along the proton transfer pathways in DdH and CpI, by fully taking into account the solvent and the protein environment. Quantum mechanical (QM) calculations at the density functional theory (DFT) level and QM/MM (molecular mechanics) molecular dynamics (MD) simulations were carried out for proton transfer pathways in DdH and CpI. The results supported the presumed biocatalytic mechanism, as compared to a mechanism where the proton binds at the Fe_p [9]. The results are also consistent with our experimental data on hydrogen production for mutated enzymes of CpI, although quantitative energy barrier estimations of the proton transfer in mutated enzymes that do not exhibit hydrogen production will require accurate free energy calculations and long time simulations for appropriate sampling, beyond the scope of this investigation. At the same time, our MD simulations and experimental confirmation of the assumed mechanism, not explored so far, established, in part, the first stage of a validated approach for future exploration of hydrogenases for hydrogen production and possibly also biomimetic analogs.

2. Computational methods

DFT calculations were carried out at the PBE [40]/6–31 + G** level, as implemented in Gaussian 03 [41]. To account for the effects of protein and solvent, QM/MM MD simulations [42] were performed, linking quantum and empirical force field simulations according to the protocol applied, as described in the following. Partial charges, energies and forces were calculated for the QM region, but no QM MD calculations directly carried out. The protein and solvent system was first relaxed by running the simulation for 1 ps at 10 K (step size 1 fs), and thereafter equilibrated for 1 ps at 300 K (step size 1 fs). In both relaxation and equilibration, coordinates of the atoms in the QM region were updated every 100 fs. After equilibration, MD simulations were performed for 1 ps at 300 K, unless indicated otherwise, updating forces and coordinates in both the QM and the MM regions at each step. The standard surface constrained all-atom solvent [43] model and the local reaction field [44] for a long-range treatment [45] were applied.

Coordinates of the protein data bank structures, namely of 1hfe (DdH) and 3c8y (CpI), were used as starting configurations in the calculations. The entire protein, consisting of the protein and solvent, was spherical and divided into four regions. Region 1 comprised of the active site cluster and side-chain groups of the proton pathway, modeled at the PBE/6–31 + G** level, with hydrogens added at the boundary of the C—C bond between the QM and MM regions. Because a force field for the [4Fe—4 S] cubane cluster was not available, all [4Fe—4 S] clusters and ligands were kept fixed, with a separate QM calculation for each cluster carried out for the atomic partial charges using the ESP [46] method. Region 2 comprised of unconstrained protein atoms and explicit water molecules of up to 25 Å from the center of region 1. This region was treated empirically by the ENZYMIX force field, as implemented in MOLARIS [47]. Lys, Arg, Asp, Glu were charged, unless otherwise indicated, in order to capture inherent interactions and enable qualitative comparison to experimental hydrogen production activity observations. In future work, for quantitative comparison with experimentally observed results upon mutation, screening effects will be fully explored. Region 3 consisted of a 2 Å shell of Langevin dipoles, and region 4 comprised a dielectric continuum beyond region 3, accounting for bulk effects.

3. Results and discussion

Analysis of proton transfer characteristics was based on pathways derived from proximate amino acid residues that can potentially be involved in hydrogen bonding. The DdH X-ray crystal structure would suggest that the pathway to DTMA in the $[Fe—Fe]_H$ sub-cluster consists of Glu159 → Ser198 → Glu156 → water460 → Cys178 → DTMA, where Glu159 and Glu156 are located in the helix, Cys178 in a separate loop, and water460 amid Cys178 and Glu156 (determined from relevant distances, i.e., O_ε(Glu159)–O_γ(Ser198) – 2.59 Å; O_γ(Ser198)–O_ε(Glu156) – 3.50 Å; O_ε(Glu156)–O(water460) – 2.67 Å; O(water460)–S(Cys178) – 3.37 Å; S(Cys178)–N(DTMA) – 3.23 Å; see Fig. 1). Similarly, for CpI, in the path (Glu282 → Ser319 → Glu279 → water612 → Cys299), Glu282 and Glu279 are in a helix, Cys299 in a loop, and water612 amid Cys299 and Glu279. The distances are: (O_ε(Glu282)–O_γ(Ser319) – 2.96 Å; O_γ(Ser319)–O_ε(Glu279) – 3.44 Å; O_ε(Glu279)–O(water612) – 3.06 Å; O(water612)–S(Cys299) – 3.20 Å; S(Cys299)–N(DTMA) – 3.46 Å). Previously it was suggested [8,22,23,28–32] that the $[Fe—Fe]_H$ sub-cluster undergoes three oxidation forms, namely, $[Fe^I—Fe^I]$, $[Fe^I—Fe^{II}]$, and $[Fe^{II}—Fe^{II}]$ in the catalytic proton reduction cycle. We therefore assumed that the first proton transfer to the $[Fe—Fe]_H$ sub-cluster takes place in its reduced state ($[Fe^I—Fe^I]$), followed by electron transfer, and then the second proton transfer occurs.

Proton transfer from the thiol of Cys178 to DTMA was first investigated for model compounds of the isolated active site (I and II) at the PBE/6–31 + G** level, in order to assure that the QM region in the simulations is appropriately selected. I comprised of the $[2Fe]_H$ sub-cluster, —CH_2SH of Cys178, and —CH_2S of the Cys that bridges to

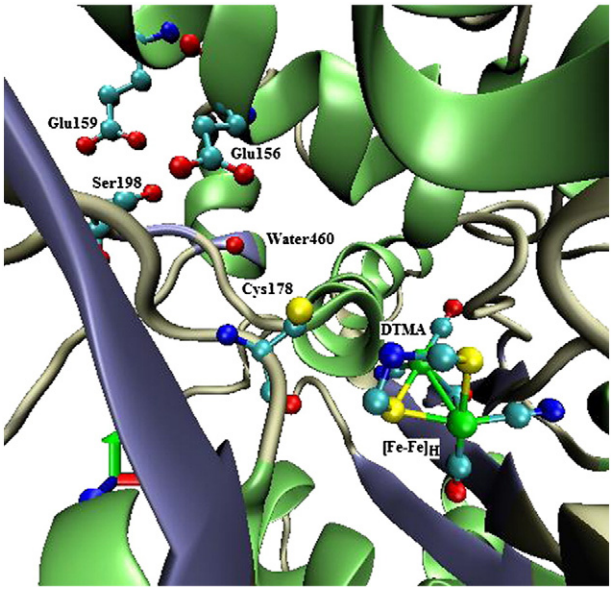

Fig. 1. Amino acid residues that comprise the proton transfer pathway in DdH [5].

the cubane cluster. Initial atomic coordinates were taken from the DdH X-ray crystal structure (PDB 1hfe). To minimize unrealistic distortions, positions of the terminal carbon atoms (capped by hydrogens) were kept fixed. In addition, a larger system was studied (II) that included two water molecules neighboring Cys178, two peptide groups forming hydrogen bonds with the two CN of the HC, the side chain of Lys237 (forming a hydrogen bond with the CN of the HC), and its nearby Glu240. Phe296 and Pro203 were also included due to spatial constraints on the CO of the HC. The results for model compounds I and II are summarized in Supplementary Fig. 1 (upper and lower panel, respectively), with the first proton transfer shown on the left, and the second (Fe_d pre-protonated) shown on the right. The valence states for the $[Fe—Fe]_H$ sub-cluster were assumed to be $[Fe^{I}—Fe^{I}]$ and $([Fe^{II}—Fe^{II}]—H^{-}$ for the first and second proton transfer, respectively. In both cases, an energetically favorable change was calculated. The different values obtained for model compounds I and II cannot be directly compared because the environment modeled is not realistic due to the constrained model. Indeed, the results demonstrated the importance of appropriate inclusion of the protein environment, as described in the following.

Limitations involved in modeling enzymatic reactions and processes are well known, yet useful insight can be gained for a broad range of applications, as was reviewed [[48–50] and references therein]. The rate constant is given by (see Eq. (17) in Aqvist et al. [48]):

$$k = Fk_{TST} = F\frac{k_B T}{h} e^{-\Delta g^*/k_B T} \quad (1)$$

where k_B and h are the Boltzmann and Planck constants, respectively; k_{TST} is the transition state theory (TST) rate constant; F includes transmission coefficients [48]; while the exponential factor that includes Δg^* (free energy difference) is the most important quantity determining the rate of enzymatic processes. Free energy calculations can be rigorously carried out by the free energy perturbation (FEP) method [48]. The activation free energy in the TST expression for the rate constant can of course also be calculated by Monte Carlo sampling, as was emphasized [51]. Overall, understanding enzymatic processes is complex, requiring constant validation, for example, in comparing the FEP method and the potential of mean force (PMF) approach for ion penetration through ion channels [52]. Such simulations are very demanding computationally and require long time computations. The rigorous FEP method will be considered in future work for proton transfer processes in CpI to enable better understanding of the effects of mutation. However, the QM/MM MD simulations described below for the case of almost barrierless transfer has established, in part, the first stage of a validated approach for future exploration of hydrogenases for hydrogen production, possibly also biomimetic analogs.

Results of the full QM/MM MD simulations for the first proton transfer from Cys178 to DTMA are shown in Fig. 2(a). The QM region included $—CH_2SH$ of Cys178, the $[Fe—Fe]_H$ sub-cluster, as well as the Cys thiolate group that covalently bridges the $[Fe—Fe]_H$ sub-cluster and the cubane cluster in the HC. The $[Fe—Fe]_H$ sub-cluster is in the reduced state $[Fe^{I}—Fe^{I}]$. In the first snapshot, the $r_{H\text{-}S(C178)}$ and $r_{H\text{-}N(DTMA)}$ distances of the relaxed initial structure were 1.410 Å and 2.382 Å, respectively, showing that the proton was bound to the sulfur of Cys178. About 200 fs thereafter, $r_{H\text{-}S(C178)}$ and $r_{H\text{-}N(DTMA)}$ changed to 1.628 Å and 1.284 Å, respectively, indicating that the proton moved amid S(C178) and N(DTMA). At 19 fs after the second snapshot, $r_{H\text{-}S(C178)}$ and $r_{H\text{-}N(DTMA)}$ changed to 1.935 Å and 1.063 Å, respectively, completing the first proton transfer process. The second proton transferred from Cys178 to DTMA (Fe_d is now pre-protonated) is shown in Fig. 2(b), assuming a $[Fe^{I}—Fe^{II}]—H^{-}$ state. In the three snapshots, distances of the proton to S(C178) were 1.410 Å (0 fs), 1.758 Å (70 fs), and 1.954 Å (78 fs), respectively. The distance of the proton to N(DTMA), of 2.882 Å (0 fs), changed to 1.200 Å after 70 fs,

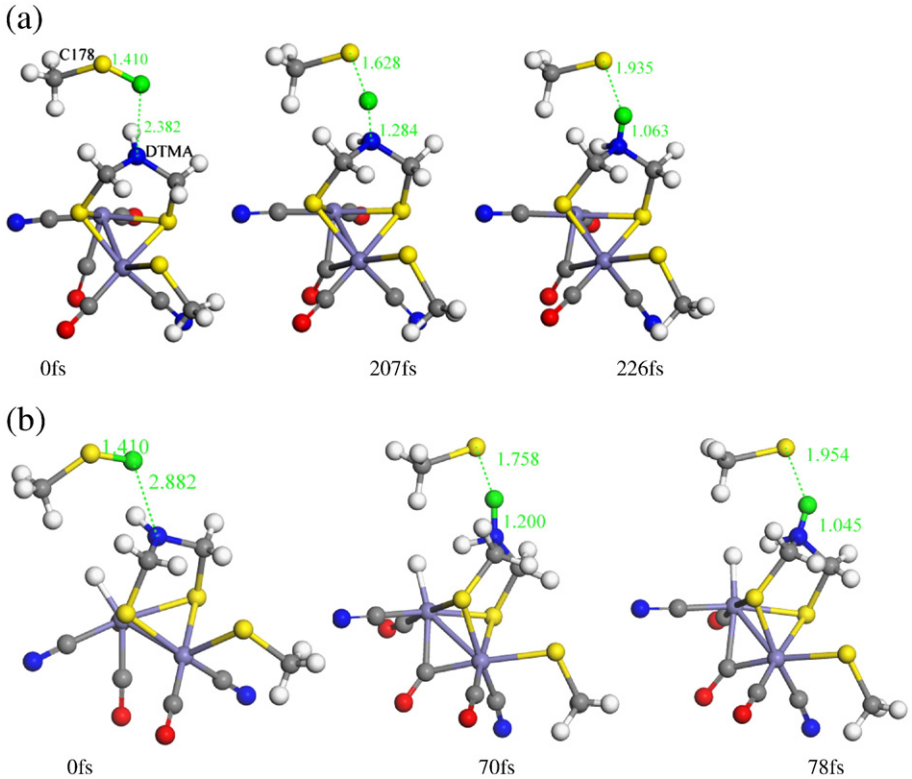

Fig. 2. Proton transfer from Cys178 to DTMA in DdH: Selected snapshots (only QM region shown) of (a) first and (b) second proton transfer; protons involved in the proton transfer are in green.

and to 1.045 Å after 78 fs. Fast de-protonation of the Cys178 thiol and consequent protonation of the DMTA amine was demonstrated by the QM/MM MD trajectories, as well as by the downhill potential energy profile obtained in examining model compounds (I and II). These results show that the amine readily "captures" a proton from the Cys178 thiol when the $[Fe—Fe]_H$ sub-cluster is in the appropriate oxidation state. In combination with the previously reported low barrier of proton transfer from DTMA to Fe_d for model compounds [22,23,28–32], it seems that DTMA easily transfers a proton from the Cys to Fe_d. In the following discussion, in simulation of the proton transfer along the proton pathway, the thiol group of Cys178 was thus assumed to be de-protonated.

Next, we studied the proton transfer within the pathway to Cys178 in DdH. Note that PBE/6–31 + G** calculations without the protein environment showed that the proton transfer from Glu159 (C_2H_5COOH) to Glu156 ($C_2H_5COO^-$) via Ser198 (—CH_2OH), and from

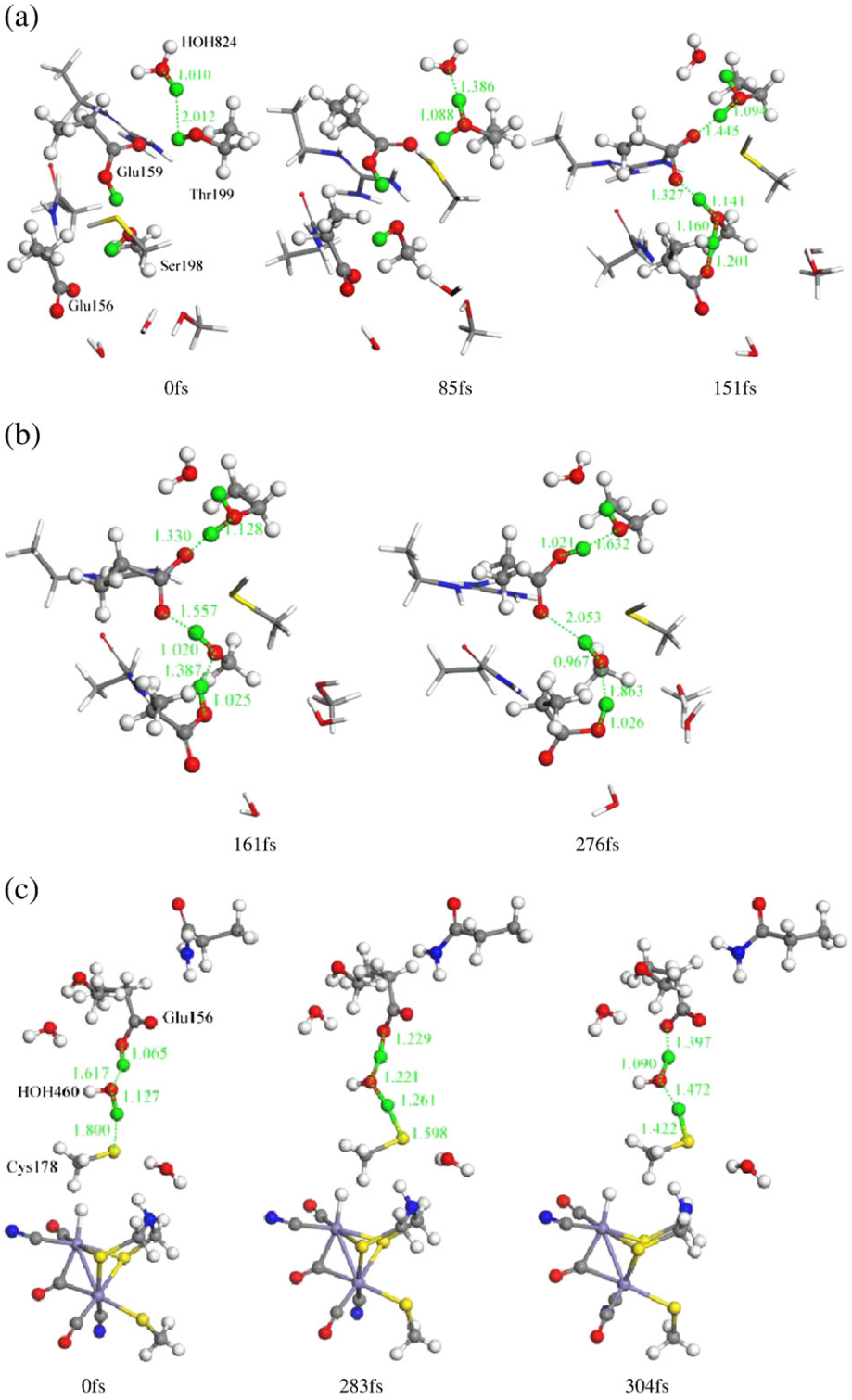

Fig. 3. Proton transfer along the pathway in DdH: Selected snapshots (only QM region shown) (a) from Glu159 to Glu156; (b) from Glu156 to Cys178; protons involved in the proton transfer are in green.

Glu156 (C_2H_5COOH) to Cys178 (—CH_2SH) via water460, have low barriers of less than 1 kcal/mol, within the accuracy of the computational method (see structures in Supplementary Figs. 2 and 3, respectively). Consequently, the proton transfer pathway was examined in two separate steps. First, in QM/MM MD simulations of the proton transfer from Glu159 to Glu156 via Ser198, the QM region included side-chain groups of Glu159 (C_2H_5COOH), Glu156 ($C_2H_5COO^-$) and Ser198 (CH_3OH), along with neighboring polar amino acid residues and water molecules, i.e., Gln174 ($C_2H_5CONH_2$), Ser177 (—CH_2OH), Thr199 (CH_2OHCH_3), Cys200 (—CH_2SH), water424, water460, water824, and charged Arg163 ($C_3H_7NHC(NH)NH_2$), with the water824 moiety protonated. Gln174 is located in the same loop as Cys178, and Arg163 in the same loop as Glu159 and Glu156. Fe_d was assumed protonated. Selected QM region snapshots from the full system's QM/MM MD simulations are shown in Fig. 3(a). It is indicated that after 85 fs the proton was transferred from water824 to Thr199, where $r_{H\text{-}O\gamma(T199)} = 1.088$ Å. At 151 fs, the proton initially bound to Glu159 moved amid Glu159 and Ser198, with values of $r_{H\text{-}O\varepsilon(E159)}$ and $r_{H\text{-}O\gamma(S198)}$ of 1.327 Å and 1.141 Å, respectively. Meanwhile the proton bound to Ser198 moved in between Ser198 and Glu156, with values of $r_{H\text{-}O\gamma(S198)}$ and $r_{H\text{-}O\varepsilon(E156)}$ of 1.160 Å and 1.201 Å, respectively. After 161 fs, the distances $r_{H\text{-}O\varepsilon(E159)}$ and $r_{H\text{-}O\gamma(S198)}$ changed to 1.557 Å and 1.020 Å, and $r_{H\text{-}O\gamma(Ser198)}$ and $r_{H\text{-}O\varepsilon(Glu156)}$ to 1.387 Å and 1.025 Å, respectively, completing two concerted proton transfer events. Specifically, the proton initially bound to Glu159 moved to Ser198, while another proton bound to Ser198 moved to Glu156. After 276 fs, the proton initially bound to Thr199 transferred to Glu159, with distances $r_{H\text{-}O\gamma(Thr199)}$ and $r_{H\text{-}O\varepsilon(Glu159)}$ of 1.632 Å and 1.021 Å, respectively, while $r_{H\text{-}O\gamma(Ser198)}$ further increased, from 1.387 Å to 1.863 Å.

In the next stage, proton transfer from Glu156 to Cys178 via water460 was investigated. The QM region included side-chain groups of Glu156, Cys178 and water460, as well as of proximate Gln174, Ser198, water424 and 455, and the $[Fe—Fe]_H$ sub-cluster. Glu159, included in the MM region, was treated as neutral. Selected QM region snapshots from the QM/MM MD simulations are shown in Fig. 3(b). Specifically, after 283 fs, values of $r_{H\text{-}O(E156)}$ and $r_{HO(water460)}$ changed to 1.229 Å and 1.221 Å, respectively, showing that the proton initially bound to Glu156 moved roughly amid O(Glu156) and O(water460). Simultaneously, the other proton moved from O(water460) in between O(water460) and S(Cys178), with $r_{H\text{-}O(water460)}$ and $r_{H\text{-}S(C178)}$ of 1.261 Å and 1.598 Å, respectively. At 304 fs, the first proton (initially bound to Glu156) transferred to water460, with distances of $r_{H\text{-}O\varepsilon(Glu156)}$ and $r_{H\text{-}O(water460)}$ of 1.397 Å and 1.090 Å, respectively. The second proton bound to water460, completed transfer to Cys178 with $r_{H\text{-}O(water460)}$ and $r_{H\text{-}S(Cys178)}$ of 1.472 Å and 1.422 Å, respectively.

For comparison with experimentally determined hydrogen production experiments we investigated proton transfer to the active site in the CpI enzyme. Side-chain groups of amino acid residues and water molecules that comprised the proton transfer pathway consisted of —CH_2CH_2COOH of Glu282, —CH_2OH of Ser319, —CH_2-CH_2COOH of Glu279, water612, and —CH_2SH of Cys299. Similar to

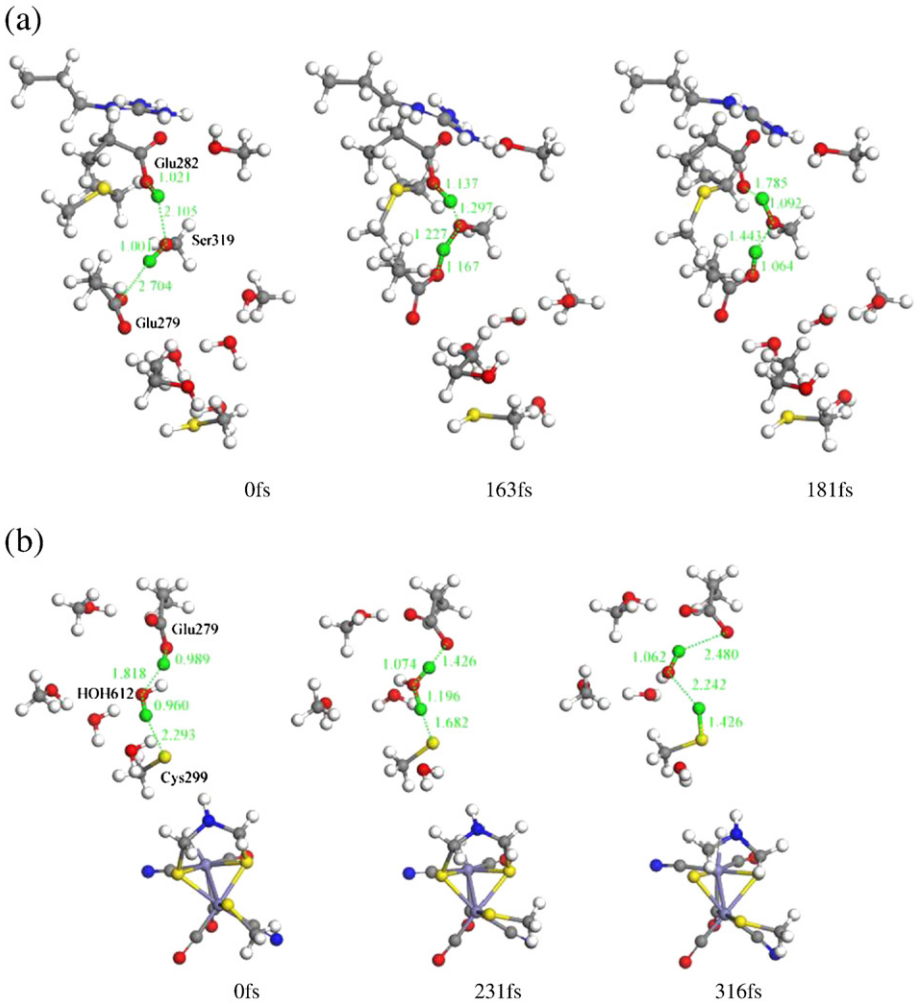

Fig. 4. Proton transfer along the pathway in CpI: Selected snapshots (only QM region shown) from (a) Glu282 to Glu279 via Ser316, (b) Glu279 to Cys299 via a water molecule; protons involved in the proton transfer are in green.

DdH, proton transfer from Glu282 to Glu279 via Ser 319 was first examined. Next, proton transfer from Glu279 to Cys299 via water612 was considered. For the first step, the QM region included in addition to Glu282, Glu279 and Ser319, also side-chain groups from neighboring polar amino acid residues and water molecules, i.e., Arg286, Cys299, Thr275, Ser298, Met295, Ser320, water598, water605 and water612. Fe_d was protonated and $[Fe^{II}—Fe^{II}]—H^-$ assumed. Selected snapshots of the QM region of the QM/MM MD simulations for the first step are shown in Fig. 4(a). After 163 fs, the proton initially bound to Glu282 moved amid Glu282 and Ser319, with $r_{H\text{-}O\varepsilon(Glu282)}$ and $r_{H\text{-}O\gamma(Ser319)}$ of 1.137 Å and 1.297 Å, respectively. The proton initially bound to Ser319 moved in between Ser319 and Glu279, with $r_{H\text{-}O\gamma(Ser319)}$ and $r_{H\text{-}O\varepsilon(Glu279)}$ of 1.227 Å and 1.167 Å, respectively. At 181 fs, $r_{H\text{-}O\varepsilon(Glu282)}$ and $r_{H\text{-}O\gamma(Ser319)}$ changed to 1.785 Å and 1.092 Å, respectively, showing that the proton initially bound to Glu282 transferred to Ser319, while $r_{H\text{-}O\gamma(Ser319)}$ and $r_{H\text{-}O\varepsilon(Glu279)}$ changed to 1.443 Å and 1.064 Å, respectively, thus the proton initially bound to Ser319 concertedly moved to Glu279.

The QM region for the second step included Glu279, water612, Cys299, [Fe—Fe] sub-cluster, Cys503, and the neighboring Ser319, Ser298, water598, and water605. Fe_d was protonated, assuming the $[Fe^{II}—Fe^{II}]—H^-$ state, with the side group of Cys299 a thiolate. The QM/MM MD results are shown in Fig. 4(b). After 231 fs, distance values of $r_{H\text{-}O\varepsilon(Glu279)}$ and $r_{H\text{-}O(water612)}$ changed to 1.426 Å and 1.074 Å, respectively, and the proton initially bound to Glu279 moved amid O(Glu279) and O(water612). The other proton, bound to water612, moved in between O(water612) and S(Cys299), with $r_{H\text{-}O(water612)}$ and $r_{H\text{-}S(Cys299)}$ of 1.196 Å, 1.682 Å, respectively. At 316 fs, the proton initially bound to Glu279 completed transfer to water612, with values of $r_{H\text{-}O\varepsilon(Glu279)}$ and $r_{H\text{-}O(water612)}$ of 2.480 Å and 1.062 Å, respectively. The proton initially bound to water612 transferred to Cys299, with distances $r_{H\text{-}O(water612)}$ and $r_{H\text{-}S(C299)}$ of 2.242 Å and 1.426 Å, respectively.

In order to gain an understanding of the role of individual amino acid residues along the proton transfer pathway, Ser319 was mutated to Ala. Simulations for 10 ps were carried out for S319A to examine the proximity of Glu282 and Glu272, which will indicate that proton transfer occurred. Distances between $O_{\varepsilon 2}$ of Glu282, and $O_{\varepsilon 1}$ and $O_{\varepsilon 2}$ of Glu279, during the QM/MM MD simulations, are shown in Supplementary Fig. 4, demonstrating fluctuations between 4.8 and 9.6 Å, clearly too large for the proton to transfer directly from Glu282 to Glu279. In addition, Cys299 was mutated to Ser and corresponding simulations were carried out for C299S. The QM region included the $[Fe—Fe]_H$ sub-cluster and Cys503, Ser299, Glu179 and water612. Analysis of the QM/MM MD simulation trajectories showed that proton transfer was not observed even after 10 ps, demonstrating an increase of the barrier compared with the wild-type enzyme, where proton transfer was readily observed. Notably, experimentally, the percent hydrogen production activity relative to the wild-type CpI was C299S 0.6% and S319A 4.6% [53]. Thus, a comparison with experimental data qualitatively validated the QM/MM MD results. However, quantitative comparison is beyond the feasibility of the computation. Yet, a validated approach has been established to further explore proton transfer characteristics in this class of hydrogenases. Interestingly, another pathway, i.e., Lys571 → water668 → water675 → water594 → Ser298 → water605 → water612 → Cys299 → DTMA (respective distances in the X-ray crystal structure 3.48, 2.80, 3.54, 3.50, 2.8, 3.01, 3.20, 3.46 Å), could be considered, however seemingly not plausible because of its inconsistency with the experimental data obtained so far for the mutated CpI enzymes.

4. Conclusion

In this work, proton transfer from the protein surface to the [Fe—Fe] sub-cluster in DdH and CpI along pathways inferred from the X-ray crystal structures were investigated by QM/MM MD simulations and model compound DFT calculations. Proton transfer in DdH from Cys178 (nearest amino acid residue in the pathway) to DTMA in the $[Fe—Fe]_H$ sub-cluster, was readily observed in the QM/MM MD trajectories, noting that $[Fe—Fe]_H$ was in the reduced state or in the mixed valence state with a protonated distal iron, as based on the supposition previously supported by experiment and computation. The results provided mechanistic consistency that has not been explored so far, specifically in the first step of proton transfer to Fe_d. A concerted mechanism is proposed, where proton transfer in DdH from Glu159 to Glu156 via Ser198 and Glu156 to Cys178 via water460 occurred, as well as from Glu282 to Glu279 via Ser319 and Glu279 to Cys299 via water612 in CpI. The rigorous FEP method will be considered in future work for proton transfer processes to the active site in CpI, to enable better understanding of the effects of mutation. These results are consistent with the experimental data on the hydrogen production activity of mutated CpI enzymes relative to the wild-type protein. Overall, the insight provided in this work, and experimental validation of the computations, are important in establishing the first stage for future exploration of proton transfer to the active site in this class of enzymes, and possibly also for biomimetic analogs.

Acknowledgments

Support from the Air Force Office of Scientific Research is gratefully acknowledged. The AFRL DSRC is acknowledged for helpful assistance. A. Warshel and his group are acknowledged for helpful discussion. The referees are gratefully acknowledged for excellent comments.

References

[1] R. Cammack, M. Frey, R. Robson, Hydrogen as a fuel: learning from nature, Taylor & Francis, London, 2001; P.M. Vignais, B. Billoud, J. Meyer, Classification and phylogeny of hydrogenases, FEMS Microbiol. Rev. 25 (2001) 455–501.

[2] L.F. Wu, M.A. Mandrand, Microbial hydrogenases: primary structure, classification, signatures and phylogeny, FEMS Microbiol. Lett. 104 (1993) 243–270; P.M. Vignais, B. Billoud, Occurrence, classification, and biological function of hydrogenases: an overview, Chem. Rev. 107 (2007) 4206–72; F.A. Armstrong, J.C. Fontecilla-Camps, Biochemistry: a natural choice for activating hydrogen, Science 321 (2008) 498–499.

[3] A. Volbeda, M.-H. Charon, C. Piras, E.C. Hatchikian, M. Frey, J.C. Fontecilla-Camps, Crystal structure of the nickel-iron hydrogenase from *Desulfovibrio gigas*, Nature 373 (1995) 580–587; Y. Higuchi, T. Yagi, N. Yasuoka, Unusual ligand structure in Ni–Fe active center and an additional Mg site in hydrogenase revealed by high resolution X-ray structure analysis, Structure 5 (1997) 1671–1680; Y. Montet, P. Amara, A. Volbeda, X. Vernede, E. Claude, E.C. Hatchikian, M. Frey, J.C. Fontecilla-Camps, Gas access to the active site of Ni-Fe hydrogenases probed by X-ray crystallography and molecular dynamics, Nat. Struct. Biol. 4 (1997) 523–526; E. Garcin, X. Vernede, E.C. Hatchikian, A. Volbeda, M. Frey, J.C. Fontecilla-Camps, The crystal structure of a reduced [NiFeSe] hydrogenase provides an image of the activated catalytic center, Structure 7 (1999) 557–566; P.M. Matias, C.M. Soares, L.M. Saraiva, R. Coelho, J. Morais, J. Le Gall, M.A Carrondo, [NiFe] hydrogenase from *Desulfovibrio desulfuricans* ATCC 27774: gene sequencing, three-dimensional structure determination and refinement at 1.8 Å and modelling studies of its interaction with the tetrahaem cytochrome c3, J. Biol. Inorg. Chem. 6 (2001) 63–81.

[4] J.W. Peters, W.N. Lanzilotta, B.J. Lemon, L.C. Seefeldt, X-ray crystal structure of the Fe-only hydrogenase (CpI) from *Clostridium pasteurianum* to 1.8 Å resolution, Science 282 (1998) 1853–1858.

[5] Y. Nicolet, C. Piras, P. Legrand, C.E. Hatchikian, J.C. Fontecilla-Camps, *Desulfovibrio desulfuricans* iron hydrogenase: the structure shows unusual coordination to an active site Fe binuclear center, Structure 7 (1999) 13–23.

[6] S. Shima, E.J. Lyon, R.K. Thauer, B. Mienert, E.J. Bill, Mössbauer studies of the iron-sulfur cluster-free hydrogenase: the electronic state of the mononuclear Fe active site, J. Am. Chem. Soc. 127 (2005) 10430–10435; S. Shima, O. Pilak, S. Vogt, M. Schick, M.S. Stagni, W. Meyer-Klaucke, E. Warkentin, R.K. Thauer, U. Ermler, The crystal structure of [Fe]-hydrogenase reveals the geometry of the active site, Science 321 (2008) 572–575.

[7] E.C. Hatchikian, N. Forget, V.M. Fernandez, R. Williams, R. Cammack, Further characterization of the [Fe]-hydrogenase from *Desulfovibrio desulfuricans* ATCC 7757, Eur. J. Biochem. 209 (1992) 357–365.

[8] M.W.W. Adams, The structure and mechanism of [Fe]-hydrogenase, Biochim. Biophys. Acta 1020 (1990) 115–145.

[9] R. Cammack, Hydrogenase sophistication, Nature 397 (1999) 214–215; P.E M. Siegbahn, J.W. Tye, M.B. Hall, Computational studies of [NiFe] and [FeFe] hydrogenases, Chem. Rev. 107 (2007) 4414–4435.

[10] P.M. Vignais, B. Billoud, Occurrence, classification, and biological function of hydrogenases: an overview, Chem. Rev. 107 (2007) 4206–4272; J.W. Peters, Structure and mechanism of iron-only hydrogenases, Curr. Opin. Struct. Biol. 9 (1999) 670–676; I.P. Georgakaki, L.M. Thomson, E.J. Lyon, M.B. Hall, M.Y. Darensbourg, Fundamental properties of small molecule models of Fe-only hydrogenase: computations relative to the definition of an entatic state in the active site, Coord. Chem. Rev. 238 (2003) 255–266; V. Artero, M. Fontecave, Some general principles for designing electrocatalysts with hydrogenase activity, Coord. Chem. Rev. 249 (2005) 1518–1535; S.P. Best, Spectroelectrochemistry of hydrogenase enzymes and related compounds, Coord. Chem. Rev. 249 (2005) 1536–1554; M. Bruschi, G. Zampella, P. Fantucci, L. De Gioia, DFT investigations of models related to the active site of [NiFe] and [Fe] hydrogenases, Coord. Chem. Rev. 249 (2005) 1620–1640; J.-F. Capon, F. Gloaguen, P. Schollhammer, J. Talarmin, Catalysis of the electrochemical H_2 evolution by di-iron sub-site models, Coord. Chem. Rev. 249 (2005) 1664–1676; X. Liu, S.K. Ibrahim, C. Tard, C.J. Pickett, Iron-only hydrogenase: synthetic, structural and reactivity studies of model compounds, Coord. Chem. Rev. 249 (2005) 1641–1652; L. Sun, B. Åkermark, S. Ott, Iron hydrogenase active site mimics in supramolecular systems aiming for light-driven hydrogen production, Coord. Chem. Rev. 249 (2005) 1653–1663; P.M. Vignais, H/D exchange reactions and mechanistic aspects of the hydrogenases, Coord. Chem. Rev. 249 (2005) 1677–1690; G.J. Kubas, Fundamentals of H_2 binding and reactivity on transition metals underlying hydrogenase function and H_2 production and storage, Chem. Rev. 107 (2007) 4152–4205; K.A. Vincent, A. Parkin, F.A. Armstrong, Investigating and exploiting the electrocatalytic properties of hydrogenases, Chem. Rev. 107 (2007) 4366–4413: J.-F. Capon, F. Gloaguen, F.Y. Pétillon, P. Schollhammer, J. Talarmin, Electron and proton transfers at di-iron dithiolate sites relevant to the catalysis of proton reduction by the [FeFe]-hydrogenases, Coord. Chem. Rev. 253 (2009) 1476–1494.

[11] O. Kruse, J. Rupprecht, K.-P. Bader, S. Thomas-Hall, P.M. Schenk, G. Finazzi, B.J. Hankamer, Improved photobiological H_2 production in engineered green algal cells, J. Biol. Chem. 280 (2005) 34170–34177.

[12] M. Bruschi, P. Fantucci, L. De Gioia, DFT investigation of structural, electronic, and catalytic properties of di-iron complexes related to the $[2Fe]_H$ subcluster of Fe-Only hydrogenases, Inorg. Chem. 41 (2002) 1421–1429; C.A. Boyke, J.I. van derVlugt, T.B. Rauchfuss, S.R. Wilson, G. Zampella, L. DeGioia, Diferrous cyanides as models for the Fe-only hydrogenases, J. Am. Chem. Soc. 127 (2005) 11010–11018; M.Y. Darensbourg, Making a natural fuel cell, Nature 433 (2005) 589–591; M.Y. Darensbourg, E.J. Lyon, X. Zhao, I.P. Georgakaki, The organometallic active site of [Fe]hydrogenase: models and entatic states, Proc. Natl. Acad. Sci. 100 (2003) 3683–3688; F. Gloaguen, J.D. Lawrence, M. Schmidt, S.R. Wilson, T.B. Rauchfuss, Synthetic and structural Studies on $[Fe_2(SR)_2(CN)_x(CO)_{6-x}]^{x-}$ as active site models for Fe-only hydrogenases, J. Am. Chem. Soc. 123 (2001) 12518–12527; C. Tard, X.Liu, S.K. Ibrahim, M. Bruschi, L. DeGioia, S.C. Davies, X. Yang, L.-S. Wang, G. Sawers, C.J. Pickett, Synthesis of the H-cluster framework of iron-only hydrogenase, Nature 433 (2005) 610–613; A. Fihri, V. Artero, M. Razavet, C. Baffert, W. Leibl, M. Fontecave, Cobaloxime-based photocatalytic devices for hydrogen production, Angew. Chem. Int. Ed. 47 (2008) 564–567.

[13] J.W. Tye, M.B. Hall, M.Y. Darensbourg, Better than platinum? Fuel cells energized by enzymes, Proc. Natl. Acad. Sci. 102 (2005) 16911–16912; A.M. Kluwer, R. Kapre, F. Hartl, M. Lutz, A.L. Spek, A.M. Brouwer, P.W.N.M. van Leeuwen, J.N.H. Reek, Self-assembled biomimetic [2Fe2S]-hydrogenase-based photocatalyst for molecular hydrogen evolution, Proc. Natl. Acad. Sci. 106 (2009) 10460–10465.

[14] S. Trohalaki, R. Pachter, Mechanism of hydrogen production in [Fe—Fe]-hydrogenase: a density functional theory study, Energ. Fuel. 21 (2007) 2278–2286.

[15] Y. Nicolet, A.L. DeLacey, X. Vernede, V.M. Fernandez, E.C. Hatchikian, J.C. Fontecilla-Camps, Crystallographic and FTIR spectroscopic evidence of changes in Fe coordination upon reduction of the active site of the Fe-only hydrogenase from *Desulfovibrio desulfuricans*, J. Am. Chem. Soc. 123 (2001) 1596–1601.

[16] A. Silakov, B. Wenk, E. Reijerse, W. Lubitz, ^{14}N HYSCORE investigation of the H-cluster of [FeFe] hydrogenase: evidence for a nitrogen in the dithiol bridge, Phys. Chem. Chem. Phys. 11 (2009) 6592–6599.

[17] A.S. Pandey, T.V. Harris, L. Giles, J.W. Peters, R.K. Szilagyi, Dithiomethylether as a ligand in the hydrogenase H-cluster, J. Am. Chem. Soc. 130 (2008) 4533–4540.

[18] W. Lubitz, E. Reijerse, M. van Gastel, [NiFe] and [FeFe] hydrogenases studied by advanced magnetic resonance techniques, Chem. Rev. 107 (2007) 4331–4365; S. P.J. Albracht, W. Roseboom, E.C. Hatchikian, The active site of the [FeFe]-hydrogenase from *Desulfovibrio desulfuricans*: I. Light sensitivity and magnetic hyperfine interactions as observed by electron paramagnetic resonance, J. Biol. Inorg. Chem. 11 (2006) 88–101.

[19] A.L. DeLacey, V.M. Fernandez, M. Rousset, R. Cammack, Activation and inactivation of hydrogenase function and the catalytic cycle: spectroelectrochemical studies, Chem. Rev. 107 (2007) 4304–4330; A.J. Pierik, M. Schmelz, O. Lenz, B. Friedrich, S. P.J. Albracht, Characterization of the active site of a hydrogen sensor from *Alcaligenes eutrophus*, FEBS Lett. 438 (1998) 231–235; Z. Chen, B.J. Lemon, S. Huang, D.J. Swartz, J.W. Peters, K.A. Bagley, Infrared studies of the CO-inhibited form of the Fe-only hydrogenase from *Clostridium pasteurianum*: I. Examination of its light sensitivity at cryogenic temperatures, Biochemistry 41 (2002) 2036–2043; A.L. De Lacey, C. Stadler, C. Cavazza, E.C. Hatchikian, V.M. Fernandez, FTIR characterization of the active site of the Fe-hydrogenase from *Desulfovibrio desulfuricans*, J. Am. Chem. Soc. 122 (2000) 11232–11233; W. Roseboom, A.L. De Lacey, V.M. Fernandez, E.C. Hatchikian, S.P.J. Albracht, The active site of the [FeFe]-hydrogenase from *Desulfovibrio desulfuricans*: II. Redox properties, light sensitivity and CO-ligand exchange as observed by infrared spectroscopy, J. Biol. Inorg. Chem. 11 (2006) 102–118.

[20] F.M. Rusnak, M.W. Adams, L.E. Mortenson, E. Munck, Mössbauer study of *Clostridium pasteurianum* hydrogenase II. Evidence for a novel three-iron cluster, J. Biol. Chem. 262 (1987) 38–41; C.V. Popescu, E. Munck, Electronic Structure of the H-cluster in [Fe]-Hydrogenases, J. Am. Chem. Soc. 121 (1999) 7877–7884; A.S. Pereira, P. Tavares, I. Moura, J.J.G. Moura, B.H. Huynh, Mössbauer characterization of the iron-sulfur clusters in *Desulfovibrio vulgaris* hydrogenase, J. Am. Chem. Soc. 123 (2001) 2771–2782.

[21] A. Le Cloirec, S.C. Davies, D.J. Evans, D.L. Hughes, C.J. Pickett, S.P. Best, S. Borg, A di-iron dithiolate possessing structural elements of the carbonyl/cyanide sub-site of the H-centre of Fe-only hydrogenase, Chem. Comm. (1999) 2285–2286.

[22] Z. Cao, M.B. Hall, Modeling the active sites in metalloenzymes: 3. Density functional calculations on models for [Fe]-hydrogenase: structures and vibrational frequencies of the observed redox forms and the reaction mechanism at the di-iron active center, J. Am. Chem. Soc. 123 (2001) 3734–3742.

[23] Z.-P. Liu, P.J. Hu, Mechanism of H_2 metabolism on Fe-only hydrogenases, J. Chem. Phys. 117 (2002) 8177–8180.

[24] Z.-P. Liu, P. Hu, A density functional theory study on the active center of Fe-only hydrogenase: characterization and electronic structure of the redox states, J. Am. Chem. Soc. 124 (2002) 5175–5182.

[25] A.T. Fiedler, T.C. Brunold, Computational studies of the H-Cluster of Fe-only hydrogenases: geometric, electronic, and magnetic properties and their dependence on the $[Fe_4S_4]$ cubane, Inorg. Chem. 44 (2005) 9322–9334.

[26] K. Nakamoto, Infrared and Raman spectra of inorganic and coordination compounds, Parts A and B, 5th ed, Wiley-Interscince, New York, 1997.

[27] A. Silakov, E.J. Reijerse, S.P.J. Albracht, E.C. Hatchikian, W. Lubitz, The electronic structure of the H-Cluster in the [FeFe]-hydrogenase from *Desulfovibrio desulfuricans*: a Q-band ^{57}Fe-ENDOR and HYSCORE study, J. Am. Chem. Soc. 129 (2007) 11447–11458.

[28] H.J. Fan, M.B. Hall, A capable bridging ligand for Fe-only hydrogenase: density functional calculations of a low-energy route for heterolytic cleavage and formation of dihydrogen, J. Am. Chem. Soc. 123 (2001) 3828–3829.

[29] G. Zampella, C. Greco, P. Fantucci, L. DeGioia, Proton reduction and dihydrogen oxidation on models of the $[2Fe]_{H\text{-cluster}}$ of [Fe] hydrogenases. A density functional theory investigation, Inorg. Chem. 45 (2006) 4109–4118.

[30] T. Zhou, Y. Mo, A. Liu, Z. Zhou, K.-R. Tsai, Enzymatic mechanism of Fe-Only hydrogenase: density functional study on H-H making/breaking at the di-iron cluster with concerted proton and electron transfers, Inorg. Chem. 43 (2004) 923–930.

[31] T. Zhou, Y. Mo, Z. Zhou, K.-R. Tsai, Density functional study on dihydrogen activation at the H-cluster in Fe-only hydrogenases, Inorg. Chem. 44 (2005) 4941–4946.

[32] C. Greco, G. Zampella, L. Bertini, M. Bruschi, P. Fantucci, L. DeGioia, Insights into the mechanism of electrocatalytic hydrogen evolution mediated by $Fe_2(S_2C_3H_6)(CO)_6$: the simplest functional model of the Fe-hydrogenase active site, Inorg. Chem. 46 (2007) 108–116.

[33] S. Trohalaki, R. Pachter, The effects of the dimethylether bridging moiety in the H-cluster of the Clostridium pasteurianum hydrogenase on the mechanism of H2 production: A quantum mechanics/molecular mechanics study, Int. J. Hydrogen Energ. 35 (2010) 13179–13185.

[34] I. Dance, Structural variability of the active site of Fe-only hydrogenase and its hydrogenated forms, Chem. Comm. (1999) 1655–1656; M. Bruschi, P. Fantucci, L. DeGioia, Density functional theory investigation of the active site of [Fe]-hydrogenases: effects of redox state and ligand characteristics on structural, electronic, and reactivity properties of complexes related to the $[2Fe]_H$ subcluster, Inorg. Chem. 42 (2003) 4773–4781; B. Maurizio, G. Claudio, K. Markus, F.U.R. Piercarlo, L. DeGioia, Influence of the $[2Fe]_H$ subcluster environment on the properties of key intermediates in the catalytic cycle of [FeFe] hydrogenases: hints for the rational design of synthetic catalysts, Angew. Chem. 48 (2009) 3503–3506.

[35] J.I. van der Vlugt, T.B. Rauchfuss, C.M. Whaley, S.R. Wilson, Characterization of a diferrous terminal hydride mechanistically relevant to the Fe-only hydrogenases, J. Am. Chem. Soc. 127 (2005) 16012–16013.

[36] F. Gloaguen, J.D. Lawrence, T.B. Rauchfuss, M. Benard, M.M. Rohmer, Bimetallic carbonyl thiolates as functional models for Fe-only hydrogenases, Inorg. Chem. 41 (2002) 6573–6582; J.L. Nehring, D.M. Heinekey, Dinuclear iron isonitrile complexes: models for the iron hydrogenase active Site, Inorg. Chem. 42 (2003) 4288–4292; G. Hogarth, I. Richards, Synthesis, crystal structure and protonation of the asymmetric iron-only hydrogenase model $[Fe_2(CO)_3(\mu\text{-pdt})\{\mu,\eta^2\text{-}Ph_2PCH_2CH_2P(Ph)CH_2CH_2\text{-}PPh_2\}]$ (pdt = $SCH_2CH_2CH_2S$), Inorg. Chem. Comm. 10 (2007) 66–70; C. Greco, M. Bruschi, P. Fantucci, L. DeGioia, Influence of a large σ-donor ligand on structural and catalytic properties of di-iron compounds related to the active site of Fe-hydrogenase–A DFT investigation, Eur. J. Inorg. Chem. (2007) 1835–1843.

[37] S. Trohalaki, R. Pachter, Mechanism of hydrogen production in [Fe-Fe]-hydrogenases: a quantum mechanics/molecular mechanics study, Int. J. Hydrogen Energ. 35 (2010) 5318–5331.

[38] J.C. Fontecilla-Camps, A. Volbeda, C. Cavazza, Y. Nicolet, Structure/function relationships of [NiFe]- and [FeFe]-hydrogenases, Chem. Rev. 107 (2007) 4273–4303.

[39] G. Zampella, P. Fantucci, L.D. Gioia, Unveiling how stereoelectronic factors affect kinetics and thermodynamics of protonation regiochemistry in [FeFe] hydrogenase synthetic models: a DFT investigation, J. Am. Chem. Soc. 131 (2009) 10909–10917.

[40] J.P. Perdew, K. Burke, M. Ernzerhof, Generalized gradient approximation made simple, Phys. Rev. Lett. 77 (1996) 3865–3868.

[41] M.J. Frisch, et al. Revision C.02 ed. Gaussian, Inc.: Wallingford CT, 2004.

[42] A. Warshel, M.J. Levitt, Theoretical studies of enzymic reactions: dielectric, electrostatic and steric stabilization of the carbonium ion in the reaction of lysozyme, Mol. Biol. 103 (1976) 227–249; J. Gao, Hybrid quantum and molecular mechanical simulations: an alternative avenue to solvent effects in organic chemistry, Acc. Chem. Res. 29 (1996) 298–305; R. Friesner, M.D. Beachy, Quantum mechanical calculations on biological systems, Curr. Opin. Struct. Biol. 8 (1998)

257–262; G. Monard, K.M. Merz, Combined quantum mechanical/molecular mechanical methodologies applied to biomolecular systems, Acc. Chem. Res. 32 (1999) 904–911; Y. Zhang, H. Liu, W. Yang, Free energy calculation on enzyme reactions with an efficient iterative procedure to determine minimum energy paths on a combined ab initio QM/MM potential energy surface, J. Chem. Phys. 112 (2000) 3483–3492; M. Field, Simulating enzyme reactions: challenges and perspectives, J. Comput. Chem. 23 (2002) 48–58.

[43] A. Warshel, G. King, Polarization constraints in molecular dynamics simulation of aqueous solutions: the surface constraint all atom solvent (SCAAS) model, Chem. Phys. Lett. 121 (1985) 124–129.

[44] G. King, A. Warshel, Investigation of the free energy functions for electron transfer reactions, J. Chem. Phys. 93 (1990) 8682–8692.

[45] Z.T. Chu, J. Villa, M. Strajbl, C.N. Schutz, A. Shurki, A. Warshel, 9.05 ed. Univ. Southern California: Los Angeles, 2004.

[46] U.C. Singh, P.A. Kollman, An approach to computing electrostatic charges for molecules, J. Comput. Chem. 5 (1984) 129–145; B.H. Besler, K.M. Merz, P.A. Kollman, Atomic charges derived from semiempirical methods, J. Comput. Chem. 11 (1990) 431–439.

[47] F.S. Lee, Z.T. Chu, A. Warshel, Microscopic and semimicroscopic calculations of electrostatic energies in proteins by the POLARIS and ENZYMIX programs, J. Comput. Chem. 14 (1993) 161–185; MOLARIS 9.05 ed.; University of the Southern California: Los Angeles, 2004.

[48] J. Aaqvist, A. Warshel, Simulation of enzyme reactions using valence bond force fields and other hybrid quantum/classical approaches, Chem. Rev. 93 (1993) 2523–2544.

[49] P. Kollman, Free energy calculations: applications to chemical and biochemical phenomena, Chem. Rev. 93 (1993) 2395–2417.

[50] J. Gao, S. Ma, D.T. Major, K. Nam, J. Pu, D.G. Truhlar, Mechanisms and free energies of enzymatic reactions, Chem. Rev. 106 (2006) 3188–3209.

[51] J. Villa, A. Warshel, Energetics and dynamics of enzymatic reactions, J. Phys. Chem. B 105 (2001) 7887–7907.

[52] M. Kato, A. Warshel, Through the channel and around the channel: validating and comparing microscopic approaches for the evaluation of free energy profiles for ion penetration through ion channels, J. Phys. Chem. B 109 (2005) 19516–19522.

[53] A.J. Cornish, G. Hong, R. Pachter, E.L. Hegg, in preparation.